Influence of the Prandtl Number on Wall-to-Fluid Thermal Transfer Rate in a Cubic Cavity

Bernardo Alan de Freitas Duarte[1] [ID] · **Ricardo Serfaty[2]** · **Aristeu da Silveira Neto[1]**

Abstract

The present paper describes a detailed qualitative and quantitative study of the impacts of the overall Prandtl number on the wall-to-fluid thermal transfer mechanisms in two-phase flows using CFD. The physical model consisted of a bubble inside a cubic cavity subjected to the gravity acceleration and to a non-isothermal field. The variables studied in the present investigation were the size of the bubble radius and the overall Prandtl number of flow. The variations of the overall Prandtl number of the flow and the bubble size were evaluated in order to understand their impact on the spatial mean Nusselt number using a computational fluid dynamics model. The bubble size was controlled modifying the bubbles' initial radius in the computational simulations and the overall Prandtl number was computed according to the Prandtl number of each phase and its volume fraction. Several computational simulations were performed and the numerical model employed in these simulations were validated with previous numerical results in the literature. The present paper reported the influence of the overall Prandtl number on regulating the thermal transfer rate in the classical problem of a differentially heated cavity. According to the numerical results, the introduction of a dispersed phase in single-phase problems may increase or reduce the thermal transfer rate, depending on the overall Prandtl number. The influence of the bubble size has also played an important role in the variations of the thermal transfer rate, since the bubble movement in the domain was modified according to to the size of this radius, changing the distance between the walls and the dispersed phase. Finally, the generally accepted hypothesis elaborated from the literature regarding the increase of the thermal transfer rate due to the introduction of bubbles in single-phase flows has failed in the cubic cavity configuration from the present research.

Keywords Nusselt number · Oberbeck–Boussinesq approximation · Computational fluid dynamics (CFD) · Natural convection

✉ Bernardo Alan de Freitas Duarte
be.duarte@hotmail.com

[1] School of Mechanical Engineering, Federal University of Uberlândia, Av. João Naves de Ávila, 2121, Bloco 5P, Uberlândia, Minas Gerais 38400-902, Brazil

[2] Petrobras, Rio de Janeiro, 21941-915, Brazil

🦋 Springer

1 Introduction

The influence of the Prandtl number on wall-to-fluid thermal exchange mechanisms in single-phase flows is widely described in the literature, namely the augmentation of the Prandtl number causes the increasement of the thermal transfer rate. For two-phase flows, wall-to-fluid thermal transfer mechanisms is yet few understood due to the number of variables affecting the flow dynamics, such as bubble's shape, turbulence, number of bubbles, quantity of dispersed phase fraction in the domain, bouyancy effects, and several other factors which could contribute to the modification of the thermal transfer rate of a two-phase flow problem. Investigations using a simple configuration and isolating other factors affecting the thermal transfer mechanisms may be important to quantify the relevance of a particular factor pertinent to the wall-to-fluid thermal transfer. Benchmarks using CFD in well-known geometries and considering simplified assumptions of physical conditions may provide key information for complex problems. Therefore, the present paper reports an extensive quantitative and qualitative study of the influence of the overall Prandtl number and the bubble size on the wall-to-fluid thermal transfer rate in two-phase flows in the classical problem of a differentially heated cavity.

The thermodynamic effects of the addition of bubbles to a single-phase flow have been widely described in several experimental and numerical studies in the literature. According to Deen and Kuipers [1], it is generally agreed that the introduction of a gas into a liquid enhances the turbulence in the medium and thus increases the thermal transfer rate to immersed surfaces. Deen and Kuipers [1] additionally defend the thesis that higher gas velocities enhance even more the thermal transfer rate. Deckwer [2] suggested that the presence of bubbles can increase the thermal transfer rate in a gas–liquid bubble column by more than one order of magnitude. Oresta et al. [3] studied the thermal transfer mechanisms in the case of Rayleigh–Bénard convection in a liquid with vapor bubbles. They concluded that the presence of bubbles had a profound effect on the structure of the flow and on the calculated Nusselt number. Deen and Kuipers [1] found that the passage of a bubble in a vertical channel increased the local thermal transfer from a hot wall. Tamari and Nishikawa [4] reported that the presence of bubbles increased the convection due to the addition of a bouyancy force. Dabiri and Tryggvason [5] studied turbulent bubbly flow and reported that the presence of bubbles increased the mixing and reduced the temperature difference between the hot wall and the bulk of the flow. They found that the Nusselt number increased by 60% when bubbles were included in the domain (considering 3% of volume fraction). According to Dabiri and Tryggvason [5], the presence of moving bubbles generally increases the local thermal transfer. Bukhari et al. [6] studied natural convection for a two-phase flow and concluded that thermodynamic patterns, such as the thermal exchange at the interface, may be directly affected by some hydraulic patterns, such as the velocity field. They concluded that the turbulent structures in the air and water phases played an important role in enhancing the thermal and mass transfer rates. Chandra and Chhabra [7] presented a quantitative analysis of the influence of the Prandtl and the Grashof numbers on single-phase flows, demonstrating the importance of the Prandtl number in regulating the thermal transfer rate for immersed surfaces in single-phase flows.

Although the literature has obtained, in general, higher wall-to-fluid thermal transfer coefficients in two-phase flows compared to single-phase flows, quantitative analysis or conclusions elucidating the causes of the numerical or experimental results previously obtained are scarce. In addition, some studies have presented opposite results, such as Qiu et al. [8], who found a reduction in the thermal transfer rate on including bubbles in the flow.

It is thus imperative to examine the thermal transfer characteristics using dimensionless parameters in order to establish general conclusions and to improve the understanding of the mechanisms underlying thermal transfer. In the present work, computational simulations of single-phase and two-phase flows are presented in order to evaluate the relation between the Prandtl number and the thermal transfer rate in a cubic cavity. The influence of the bubble size is also evaluated in the present paper. Since information about the thermal transfer rate in single-phase and two-phase flows is crucial to several industrial processes as well as to various equipment employed in engineering applications, the present paper may guide and improve the efficiency of the thermal transfer operations. Finally, the present paper presents new insights into the thermal transfer mechanisms, opening new research opportunities related to non-isothermal two-phase flows.

2 Physical Model

The physical model used in the present paper consists of a three-dimensional cavity where the flow is subjected to thermal effects. A cavity is used as physical model due to its simple geometry [9] and presence in several industrial applications [10].

The analysis conducted in the present paper was performed while imposing constant values for the Grashof number and different values of the Prandtl number and bubble radius. The Grashof number represents the ratio of buoyancy to viscous force on a fluid and is defined according to the following equation [11]:

$$Gr = \frac{g\beta(T_s - T_\infty)L^3}{\nu^2} \tag{1}$$

where g is the acceleration due to gravity, β is the volumetric expansion coefficient, T_s is the temperature at the reference surface, T_∞ is the temperature far away from the surface of reference, L is the characteristic length, and ν is the kinematic viscosity. The Prandtl number defines the ratio of momentum diffusivity to thermal diffusivity and is given by the following expression [11]:

$$Pr = \frac{\mu Cp}{k} \tag{2}$$

where Cp is the specific heat, μ is the dynamic viscosity, and k is the thermal conductivity.

In the analysis of the simulations, the overall Prandtl number (Pr_{ove}) of the flow was calculated, defined by the following expression:

$$Pr_{ove} = \varphi Pr_{dis} + (1 - \varphi)Pr_{con} \tag{3}$$

where φ is the volume fraction of the dispersed phase in the domain, Pr_{dis} is the Prandtl number for the dispersed phase, and Pr_{con} is the Prandtl number for the continuous phase.

The simulations were performed employing the Oberbeck–Boussinesq approximation (OB) in a cubic cavity with a characteristic length L. The characteristic length L was equal to 1.0 m in all the simulations. Bouyancy and gravity forces were neglected.

The domain boundaries were named using geographic orientation, namely north, south, east, west, bottom, and top faces. A schematic image of the configuration of the cavity used in the present work and the names of the domain boundaries are presented in Fig. 1.

Null velocity and null pressure gradient were imposed at all the domain faces. The acceleration of gravity was assumed to be 9.81 m/s^2. The east and west wall were given an
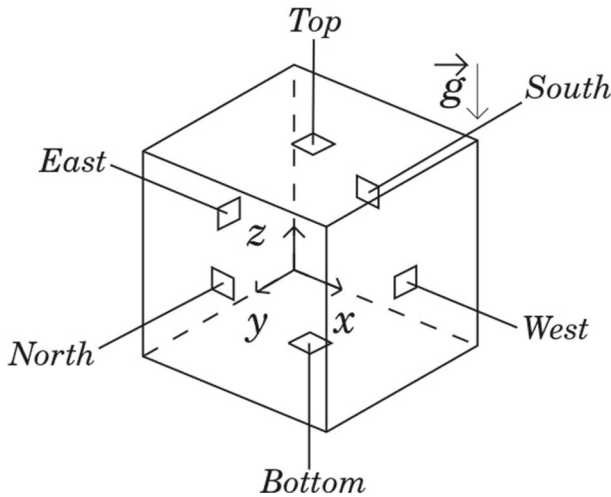
Fig. 1 Physical model with the names of the domain boundaries

imposed high (T_h) and low (T_l) temperature, respectively; and the other walls were considered adiabatic. The initial conditions for all the simulations were: null velocity, null pressure, and temperature of T_l in all the domain.

The prediction of the thermal exchange rate between the flow and the east wall (kept at a fixed temperature T_h) was conducted over the entire time of the simulations. The thermal transfer rate was calculated using the spatial mean Nusselt number at the east wall. The Nusselt number (Nu) represents the ratio between the conductive and convective thermal transfer processes; therefore, when $Nu < 1$, conduction is predominant, and when $Nu > 1$, the advection effects are more predominant than conduction [12]. The Nusselt number may be defined by the following expression [1]:

$$Nu = \frac{L}{\Delta T} \frac{\delta T}{\delta x}|_{x=0} \tag{4}$$

where T is the temperature and ΔT is the temperature difference between the east and west walls.

All the analysis conducted in the present paper employed the calculation of the spatial mean Nusselt number ($\bar{N}u$) at the east wall. The spatial mean Nusselt number was defined by the following expression:

$$\bar{N}u = \frac{\sum_1^n Nu}{n} \tag{5}$$

where n is the number of computational cells at the east wall.

In two-phase flows, the bubble is constantly subjected to relatively high velocities due to the dynamics of the flow, causing the bubble to move and its shape to deform over time. In order to preserve the spherical shape of the bubbles, all the two-phase flow simulations were performed while imposing a constant and relatively high surface tension coefficient, which was defined as 30.0 N/m. This was imposed since Dabiri and Tryggvason [5] reports the influence of the bubble shape on the thermal transfer dynamic; therefore, the shape of the bubble was not studied in the present paper. Since $\frac{Gr}{Re^2} >> 1$, forced convection may be neglected.

3 Mathematical Model

The continuity, momentum, and energy equations were solved employing the following expressions:

$$\nabla.\mathbf{v} = 0, \tag{6}$$

where $\mathbf{v}$ is the fluid velocity.

$$\rho_0 \frac{D\mathbf{v}}{Dt} = -\nabla p + (\rho - \rho_0)\mathbf{g} + \mu\nabla^2\mathbf{v} + \overrightarrow{f}_{st}(\mathbf{x}, t), \tag{7}$$

where t is the time, p is the pressure, ρ_0 is the specific mass of reference, and $\overrightarrow{f}_{st}$ is the source term used to model the effects of the force of surface tension.

$$\rho_0 Cp \frac{DT}{Dt} = \nabla.(k\nabla T). \tag{8}$$

where α is the thermal diffusivity. The Oberbeck–Boussinesq approximation was employed in order to model the effects of a variable specific mass. The following thermodynamic relation was employed in the momentum equation to compute these effects: a temperature function [11]

$$(\rho - \rho_0)\mathbf{g} = -\rho_0\beta(T - T_0)\mathbf{g} \tag{9}$$

where T_0 is the temperature of reference.

Finally, the effects of surface tension were included in the formulation using the model of Brackbill et al. [13]. This model specifies the force of surface tension per unit of volume as

$$\overrightarrow{f}_{st}(\mathbf{x}, t) = \frac{\rho\sigma\kappa\nabla\phi}{\frac{1}{2}(\rho_{liq} + \rho_{vap})}, \tag{10}$$

where σ is the surface tension coefficient and $kappa$ is the curvature.

4 Numerical Model

The partial differential equations were solved with a standard finite volume method on a staggered rectangular three-dimensional grid. The velocity–pressure coupling was accomplished using a two-step projection method [14] with an explicit treatment for advection terms and an implicit treatment for pressure and diffusion terms. The Barton scheme [15] was used for the spatial discretization of the advective terms. The energy equation was solved implicitly using a multigrid-multilevel solver. The transient equations were solved using the MFSim program, which has been developed over the last ten years in cooperation with a large research group and with the scientific support of Petrobras, a semi-public Brazilian multinational corporation in the petroleum industry, headquartered in Rio de Janeiro, Brazil. The turbulence modeling was performed using Large Eddy Simulation (LES) and the turbulence closure was done via the dynamic model of Germano et al. [16] and Lilly [17].

The duration of the simulations was defined according to the stabilization of the calculation of the spatial mean Nussel number at the east wall. All simulations were performed in a parallel environment in the fluid mechanics laboratory cluster at the Federal University of Uberlândia, Brazil. The code uses single and multi-block structured meshes and a variable time step. The magnitude of the allowable time step for stable calculations is determined from the convective and viscous terms. The constraint is defined according to the CFL (Courant–Friedrichs–Lewis condition) and the mesh size [18]. The tolerance of the numerical model in providing a solution to the continuity, momentum, and energy equations

was 10^{-6}. In order to ensure the incompressibility condition, the velocity divergence in each computational cell was evaluated and was not higher than 10^{-11} s^{-1} during all the performed simulations.

A volume of fluid (VOF) method [19] was applied to determine the location of the interface and the transport. VOF employs a color function $\varphi(\mathbf{x}, t)$ to indicate the fractional amount of fluid present at a certain position $\mathbf{x}$ and at time t. The color function φ is calculated using the following equation [20]:

$$\frac{\partial \varphi}{\partial t} + [\mathbf{v}_{normal} . \nabla \varphi] = 0. \tag{11}$$

The flow fluid properties were calculated based on the volume fraction of the continuos and dispersed phases, as Deen et al. [1]:

$$\rho = \varphi \rho_{dis} + (1 - \varphi) \rho_{con} \tag{12}$$

$$\mu = \varphi \mu_{dis} + (1 - \varphi) \mu_{con} \tag{13}$$

$$k = \varphi k_{dis} + (1 - \varphi) k_{con} \tag{14}$$

$$cp = \varphi cp_{dis} + (1 - \varphi) cp_{con} \tag{15}$$

The VOF method applied in the MFSim code employed the PLIC algorithm [20] and the curvature was computed using the Least Squares method [21]. The two-phase flow model was previously validated in Franco et al. [22]. In addition, spurious currents were evaluated in the latter work and it presented none relevance for even complex computational simulations of multiple ascending bubbles. For more details, the readers are invited to see the work of Franco et al. [22].

5 Validation of the Numerical Model

Two validation cases are presented in this section, namely modelling natural convection in single-phase flows (case 1) and modelling natural convection in two-phase flows (case 2).

## 5.1 Validation case 1: simulations of natural convection in single-phase flows

Natural convection simulations in a cubic cavity assuming a Rayleigh number of 1.89×10^5 were performed using OB for validation purposes. Temperature profiles were plotted and then compared with the experimental results of Krane and Jessee [23] and the numerical results of Padilla et al. [24].

A uniform temperature field was imposed on the east (T_{high}) and west (T_{low}) walls. The south and north walls were considered adiabatic, and a linear temperature field, given by the expression $T(x, y, 0) = T(x, y, L) = T_{high} - (T_{high} - T_{low})\frac{x}{L}$, was imposed on the bottom and top walls.

Two dimensionless temperature lines from inside the domain were extracted from the numerical results, namely, $T^*(x, L/2, L/2)$ and $T^*(L/2, y, L/2)$. The expression for the dimensionless temperature is given by

$$T^*(dimensionless) = \frac{T}{T_{east} - T_{west}}, \tag{16}$$

where T_{east} represents the temperature at the east wall and T_{west} represents the temperature at the west wall.
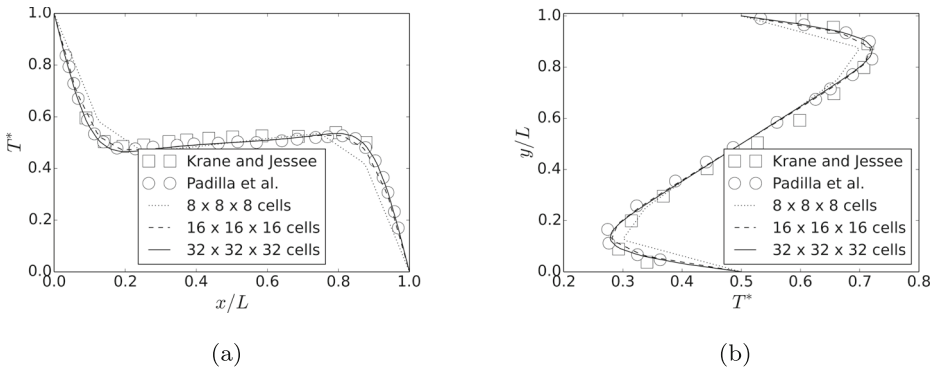
Fig. 2 Dimesionless temperature along the lines $T^*(x, L/2, L/2)$ and $T^*(L/2, y, L/2)$, for $Ra = 1.89 \times 10^5$ with OB

Figure 2a presents the dimensionless temperature along the line $T^*(x, L/2, L/2)$ for OB. Likewise, Fig. 2b presents the dimensionless temperature along the line $T^*(L/2, y, L/2)$ for OB.

The simulations using OB demonstrated good agreement with the experimental data of Krane and Jessee [23] and with the numerical data of Padilla et al. [24], as observed in Fig. 2. The numerical results from the present paper are slightly closer to those reported in the numerical work of Padilla et al. [24] than those from the experimental work of Krane and Jessee [23].

The average relative difference (ε) between the experimental data and the computed values from the present work are shown in Table 1. According to the results seen in Table 1, OB provides numerical results with low deviation from the experimental data of Krane and Jessee [23]. The maximum difference between the experimental data and OB was 7.3% for the most fine grid.

In order to present a grid quality analysis, the dimensionless temperatures obtained for the three different meshes were compared. The temperature from the line $T^*(x, L/2, L/2)$ was chosen for the comparison between the different meshes. Table 2 shows the data for $x/L = 0.2$, $x/L = 0.5$ and $x/L = 0.8$ using OB. The relative difference between two sucessive grid configurations (ψ) is also presented in Table 2.

Since the temperature field was solved using a second-order scheme, it is expected that the error found for a grid with size ζ is one-fourth that obtanied for a grid with size 2ζ. When the relative difference between the error obtained for two grids is significantly low and its values are close to the reference, it is assumed that this is a good quality grid. As seen in Table 2, the grid configuration of $32 \times 32 \times 32$ is of great quality since its values are very close to the experimental data from the literature (seen in Table 2), as well as the fact that the relative difference between the error with the coarser grid is not significant compared to

Table 1 Average relative difference (ε) between OB and the experimental data of Krane and Jessee [23]

Mesh configuration	ε (%) using OB
$8 \times 8 \times 8$	6.5
$16 \times 16 \times 16$	5.1
$32 \times 32 \times 32$	4.9

Table 2 Dimensionless temperature for OB for $x/L = 0.2$, $x/L = 0.5$ and $x/L = 0.8$ from the line $T^*(x, L/2, L/2)$

Mesh configuration	$x/L = 0.2$	$\psi(\%)$	$x/L = 0.5$	$\psi(\%)$	$x/L = 0.8$	$\psi(\%)$
$8 \times 8 \times 8$	0.51	–	0.50	–	0.49	–
$16 \times 16 \times 16$	0.47	8.51	0.50	0	0.53	7.54
$32 \times 32 \times 32$	0.46	2.17	0.50	0	0.53	0

the $32 \times 32 \times 32$ grid. Therefore, based on the numerical results obtained in the simulations presented in this section, it can be concluded that both formulations are in accordance with the literature, assuring us of the accuracy of the numerical methods employed.

5.2 Validation case 2: simulations of natural convection in two-phase flows

Natural convection in two-phase flow was simulated and validated by the calculation of the spatial mean Nusselt number at the east wall. Qiu et al. [8] presented this numerical experiment of natural convection with two-phase flow using Oberbeck-Boussinesq approximation (since the specific mass was the same for the two fluids, and the other fluid properties were different).

Null velocities and null pressure gradient were imposed to all the domain faces. The east and west walls have, respectively, a uniform high (T_h) and low temperature (T_l). The south, north, bottom and top walls are adiabatic. The fluid is at rest in initial conditions and the temperature field is uniform and igual to T_l.

The Prandtl number was set as 0.71 and Rayleigh number was 10^3 for the dispersed phase and 10^4 for continuos phase. The dispersed phase consisted of a bubble in the center of the cavity. Two values of initial bubble radius were tested, namely: $0.15L$ and $0.31L$. The wall-to-fluid thermal transfer rate was examined by means of the spatial mean Nusselt number calculation. A computational grid with one and two levels of refinement were tested and the base level presented $32 \times 32 \times 32$ cells.

The Fig. 3 shows the isotherms in the cases of a bubble initial radius of $0.15L$ and $0.31L$, respectively.
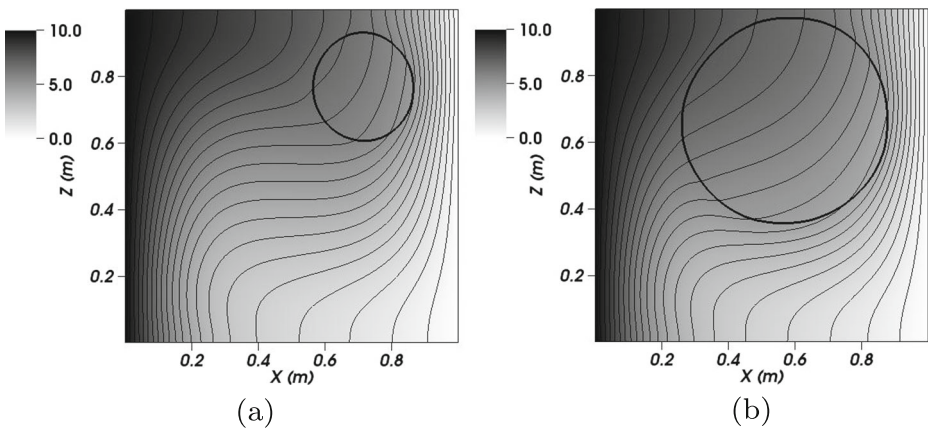
Fig. 3 Isotherms at central xz-plane for $r = 0.15L$ (**a**) and $r = 0.31L$ (**b**). Interface is represented by a contour line
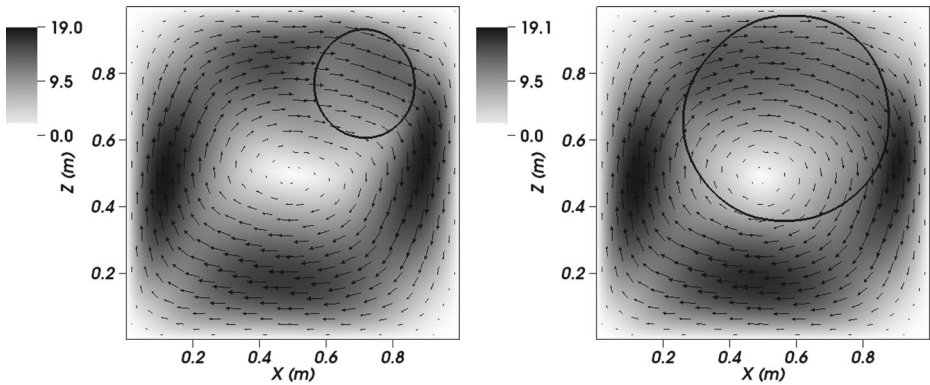
Fig. 4 Velocity field at the central xz-plane considering $r = 0.15L$ (**a**) and $r = 0.31L$ (**b**). The interface is represented by a contour line

The presence of the bubble changed significantly the thermal transfer pattern inside the cavity as shown in the Fig. 3. As seen in the Fig. 3, the isotherms tend to be more vertical inside the bubble, as found by Qiu et al. [8]. The Fig. 4 shows the clockwise movement described by the bubble inside the cavity due to thermal bouyancy effects, as previously reported by Qiu et al. [8].

A 3D visualization of the interface contour is shown in the Fig. 5.

The spatial mean Nusselt number presented good agreement with Qiu et al. [8] for the two different initial radius tested. The Table 3 shows the spatial mean Nusselt number found in the present paper and the ones found from the literature.

The introduction of a bubble with a larger radius caused the reduction of the spatial mean Nussselt number at the heated wall, similarly to the results found by Qiu et al. [8]. The influence of the Grashof number in the local thermal transfer was significantly visible in the previous table, since the overall Grashof number was lowered by the introduction of a dispersed phase, as previously stated by the literature for single-phase-flows [9].

The computational simulations of the present work were performed using a mesh with one refinement level and a base level with $32 \times 32 \times 32$ cells. since the grid configuration using one refinement level presented results with good agreement and mesh convergence was achieved with the most refined level.

(a)   (b)
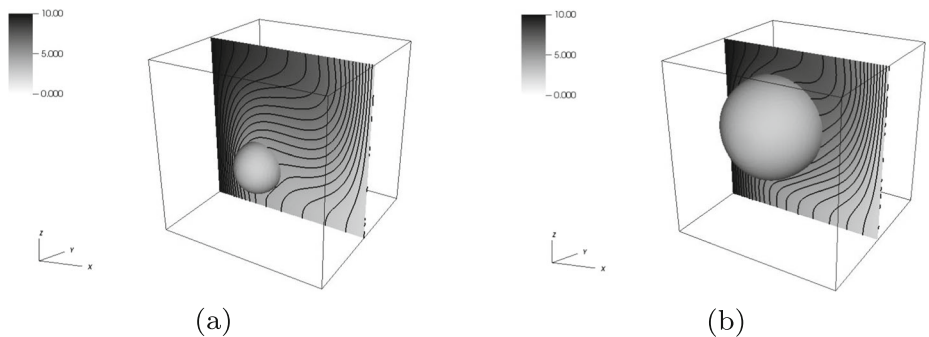
Fig. 5 Temperature and isotherms visualization for $r = 0.15L$ (**a**) and $r = 0.31L$ (**b**). The interface is represented by a contour line

Table 3 Spatial mean Nusselt number at the east wall for two values of bubble's initial radius

	Bubble radius of $0.15L$	Bubble radius of $0.31L$
Qiu et al. [8]	2.13	2.08
Present work - one refinement level	2.03	2.00
Present work - two refinement levels	2.04	2.01

## 6 Influence of the Prandtl Number on Single-Phase Flows

The literature already accepts the general hypothesis of the thermal transfer rate augmentation due to the increasement of the Prandtl number on single-phase flows. Therefore, the results shown here only confirm and illustrate the influence of the Prandtl number on the temperature field in single-phase flows.

Simulations were conducted using a Grashof number of 1.4×10^3 and two values of the Prandtl number were tested: $Pr = 0.71$ and $Pr = 7.10$. Figure 6 shows the isotherms and the temperature field for the simulations with Grashof number 1.4×10^3 and Prandtl numbers $Pr = 0.71$ and $Pr = 7.10$.

According to the Fig. 6, the Prandtl number affected the temperature field since the pattern of the isotherms was completely different between the Fig. 6a and b. The pattern of the isotherms changed a great deal as the Prandtl number changed from 0.71 to 7.1 since the isovalues of temperature became more horizontal compared to the bottom and top walls. The temperature field presents a strong stratification profile at the cavity center due to advection effects for the case of Pr=7.1 and the case with Pr=0.71 shows no stratification because of the low advection magnitude since $Nu < 1$.

The spatial mean Nusselt number was computed at the east wall and the highest thermal transfer rate was associated to the simulations with the highest value of the Prandtl number, as shown is Table 4.

According to the results found here, the Prandtl number affected the wall-to-fluid thermal transfer rate as well as the pattern of the isotherms. Next, the influence of the Prandtl number on two-phase flows is evaluated.

(a)   (b)
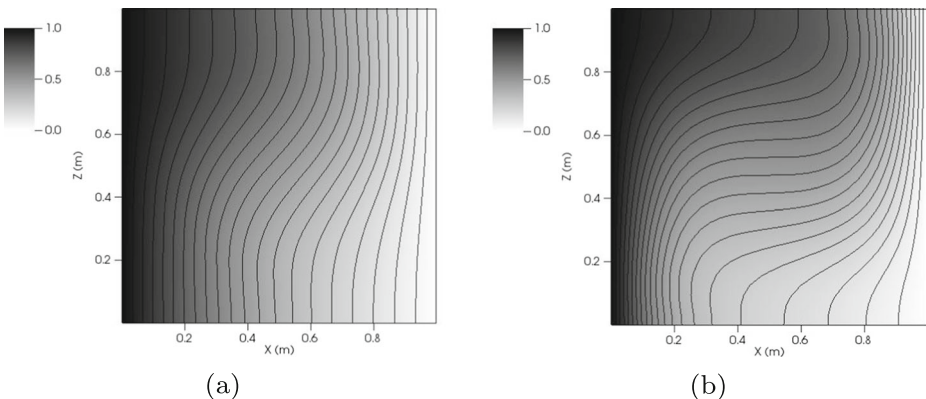
Fig. 6 Isotherms and temperature field for $Gr = 1.4 \times 10^3$ and $Pr = 0.71$ (**a**) as well as for $Pr = 7.1$ (**b**)

Table 4 Summary of the thermal transfer rate results in the single-phase flow cases

Single-phase flow	Nu
$Pr = 0.71$	1.07
$Pr = 7.1$	2.09

7 Two-Phase Flow Simulations Where the Prandtl Number of the Dispersed Phase is Higher than the Prandtl Number of the Continuous Phase

In this section, two-phase flows are investigated in the situation where the Prandtl number of the dispersed phase is higher than the Prandtl number of the continuous phase. The results of three different analyses are presented in this section, namely:

- $Pr_{dis} > Pr_{con}$ and the effects of varying the overall Prandtl number variation;
- $Pr_{dis} > Pr_{con}$ and the effects of varying the bubble size;
- $Pr_{dis} > Pr_{con}$ and the effects of varying both the bubble size and overall Prandtl number variation.

In Section 7.1, the results of two-phase flow simulations are presented, in which there was an initial bubble radius of $0.31L$ and the overall Prandtl numbers analyzed were 1.06 and 1.51. In Section 7.2, the results of two-phase flow simulations are presented, in which the overall Prandtl number was 1.06 and two bubble radii were tested: $r = 0.31L$ and $r = 0.40L$. Lastly, in Section 7.3, the results of two-phase flow simulations will be presented, in which the overall Prandtl numbers were 1.51 and 2.30 and the bubble radii were $r = 0.31L$ and $r = 0.39L$.

7.1 Simulations with $Pr_{dis} > Pr_{con}$ and the effects of variations in the overall Prandtl number

In this subsection, there will be presented the results of two-phase flow simulations with a dispersed phase with a bubble radius of $0.31L$. The Grashof number was taken equal 1.4×10^3 and the continuous phase had a Prandtl number of 0.71.

First, the Prandtl number for the dispersed phase was five times higher than in the continuous phase ($Pr_{dis} = 3.55$ and $Pr_{con} = 0.71$, leading to an overall Prandtl number of 1.06). Then, a simulation was performed considering a dispersed phase with Prandtl number ten times higher than the continuous phase ($Pr_{dis} = 7.10$ and $Pr_{con} = 0.71$, leading to an overall Prandtl number of 1.51).

Figure 7 shows the isotherms and temperature field in the two-phase flow cases with Gr=1.4×10^3 and $Pr_{ove} = 1.06$ a and $Pr_{ove} = 1.51$ b.

According to Fig. 7, the configuration of the isotherms was deeply modified inside the dispersed phase. The isotherms in Fig. 7 were not primarily vertical, since the isotherms were more horizontal inside the dispersed phase.

Figure 8 shows the evolution over time of the spatial mean Nusselt number for the single-phase case ($Pr = 0.71$), the two-phase flow case with $Pr_{ove} = 1.06$, and the two-phase case with $Pr_{ove} = 1.51$.

Figure 8 shows the severe influence of the overall Prandtl number on the spatial mean thermal transfer rate. As the overall Prandtl number increases, the spatial mean Nusselt number increases. In comparison to the single-phase case, the two-phase cases demonstrate
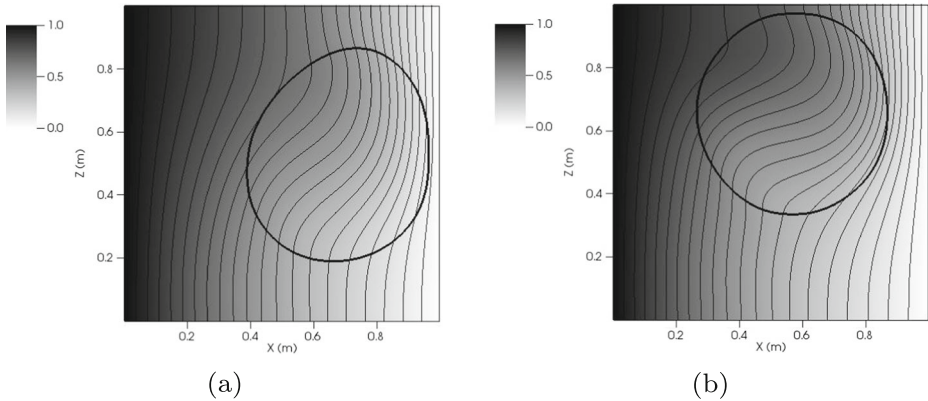
Fig. 7 Isotherms and temperature field at the central xz-plane with Gr=1.4×10^3, $Pr_{ove} = 1.06$ (**a**) and $Pr_{ove} = 1.51$ (**a**). The isotherms are represented with 20 thin isovalue contours. The thick contour represents the position of the interface. The temperature field is presented in grayscale

a significant increase in the mean thermal transfer rate due to the variation of the overall Prandtl number.

Table 5 summarizes the data related to the simulations presented in this subsection.

According to Table 5, the spatial mean Nusselt number increased as the overall Prandtl number was increased. The minimum values of the thermal transfer rate ($\bar{Nu}_{min}$ seen in Table 5) are associated to the moment when the dispersed phase was the farthest from the east wall. In addition, the maximum values of the thermal transfer rate ($\bar{Nu}_{max}$ seen in Table 5) were related to the moment when the dispersed phase was the nearest to the east
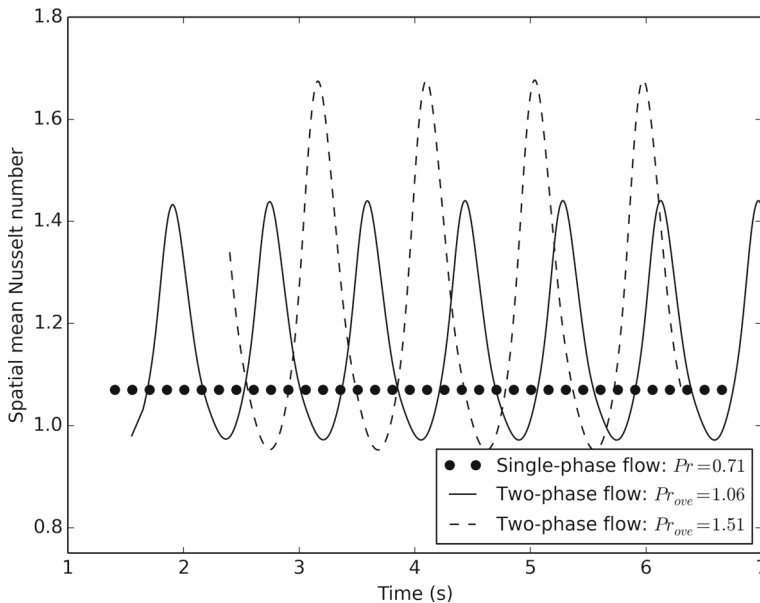
Fig. 8 Temporal evolution of the spatial mean Nusselt number for the single-phase case ($Pr = 0.71$) and two-phase flow cases with $Pr_{ove} = 1.06$ and $Pr_{ove} = 1.51$

Table 5 Summary of the thermal transfer rate results for the effect of varying the overall Prandtl number

	$\bar{N}u_{mean}$	$\bar{N}u_{min}$	$\bar{N}u_{max}$
Single-phase flow with $Pr = 0.71$	1.07	1.07	1.07
Two-phase flow with $Pr_{ove} = 1.06$	1.16	0.97	1.44
Two-phase flow with $Pr_{ove} = 1.51$	1.23	0.95	1.67

wall. Therefore, the proximity of the dispersed phase to the east wall was a important factor affecting the Nusselt number when $Pr_{dis} > Pr_{con}$.

7.2 Simulations with $Pr_{dis} > Pr_{con}$ and the effects of variations in the bubble size

In this subsection, the results of two-phase flow simulations with a dispersed phase with a bubble radius of $0.31L$ and $0.40L$ will be presented. The Grashof number was taken equal to 1.4×10^3 and the continuous phase had a Prandtl number of 0.71. The overall Prandtl number was 1.06 for both simulations ($r = 0.31L$ and $r = 0.40L$).

Figure 9 shows the temporal evolution of the spatial mean Nusselt number for the single-phase case ($Pr = 0.71$), the two-phase flow with $r = 0.31L$ ($Pr_{ove} = 1.06$), and the two-phase flow with $r = 0.39L$ ($Pr_{ove} = 1.06$).

According to Fig. 9, the spatial mean Nusselt number varied in time for both cases ($r = 0.31L$ and $r = 0.40L$). The variations of the spatial mean Nusselt number were more prominent in the case for the bubble radius of $0.31L$ compared to the case with $r = 0.40L$.

Table 6 summarizes the data related to the simulations treated in this subsection.

According to Table 6, the bubble radius directly affected the thermal transfer rate in time. The smaller bubble radius was associated to a higher maximum and mean value of
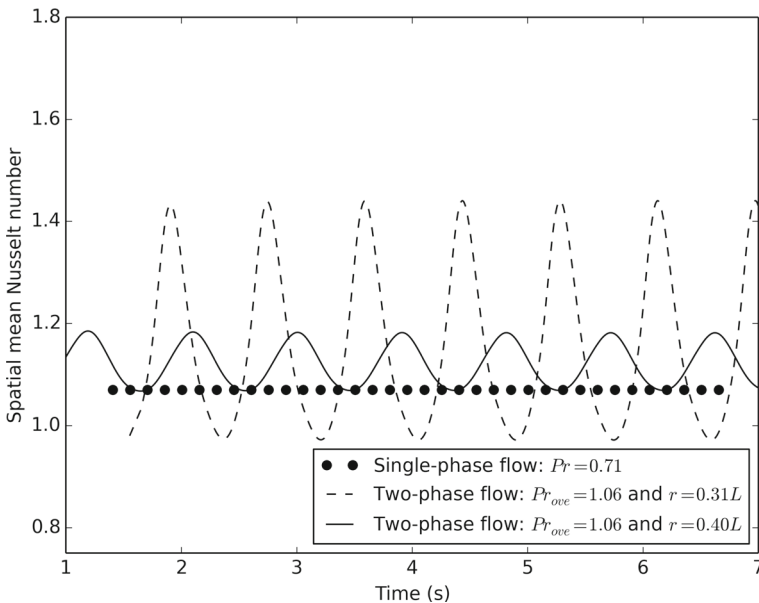
Fig. 9 Evolution of the spatial mean Nusselt number for the single-phase case ($Pr = 0.71$), two-phase flow with $r = 0.31L$ ($Pr_{ove} = 1.06$), and two-phase flow with $r = 0.40L$ ($Pr_{ove} = 1.06$)

		$\bar{N}u_{mean}$	$\bar{N}u_{min}$	$\bar{N}u_{max}$
Table 6 Summary of the effects on the thermal transfer rate of bubble size variation with the Grashof number equal to 1.4×10^3 and overall Prandtl number was 1.06	Two-phase flow with $r = 0.31L$	1.16	0.97	1.44
	Two-phase flow with $r = 0.40L$	1.12	1.07	1.18

thermal transfer rate compared to the case with larger bubble radius. According to visual observations over the simulation time, the proximity between the wall and the bubbles was higher for the case with $r = 0.31L$ in comparison to $r = 0.40L$. Therefore, the size of the bubble radius had consequences for the bubble movement inside the cavity and probably the distance effect may have promoted the difference in the Nusselt number calculations.

7.3 Simulations with $Pr_{dis} > Pr_{con}$ and the effects of simultaneous variation of the bubble size and overall Prandtl number

This subsection presents the results of two-phase flows simulations with a dispersed phase with a bubble radius of $0.31L$ and $0.39L$ and overall Prandtl numbers of 1.51 and 2.30, respectively. Here, the effects of the bubble radius size were taken into account as well as the influence of varying the overall Prandtl number.

Simulations of natural convection were performed assuming $Gr = 1.4 \times 10^3$ and $Pr = 7.1$ for the dispersed phase and $Pr = 0.71$ for the continuous phase. The simulations were performed for two different initial bubble radii, namely $r = 0.31L$ and $r = 0.39L$. The overall Prandtl number was 0.71 for the single-phase flow, 1.51 for the two-phase flow with dispersed phase with radius of $0.31L$, and 2.30 for the simulation of a two-phase flow with an spherical dispersed phase with radius of $0.39L$.

Figure 10 shows the isotherms for the two-phase cases with overall Prandtl numbers of 1.51 and 2.30.

Figure 10 illustrates the consequences of varying the overall Prandtl number on the temperature field since the isotherms were modified compared to the single-phase case. As seen in Fig. 7, inside the dispersed phase, the isotherms exhibit a deeply modified aspect since the isotherms were mainly horizontal inside the dispersed phase. In addition, the larger size

(a)   (b)
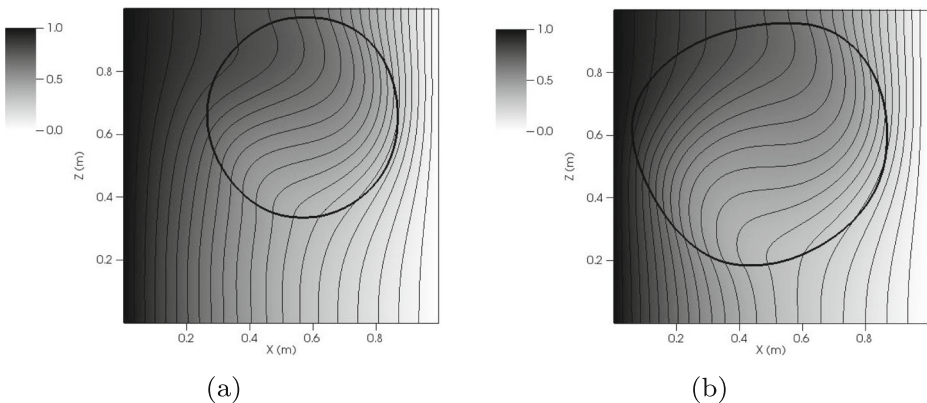
Fig. 10 Isotherms at the central xz-plane for Gr=1.4×10^3 and overall Prandtl numbers of 1.51 and 2.30. The isotherms are represented by 20 thin isovalue contours. The thick contour represents the position of the interface. The temperature field is presented in grayscale
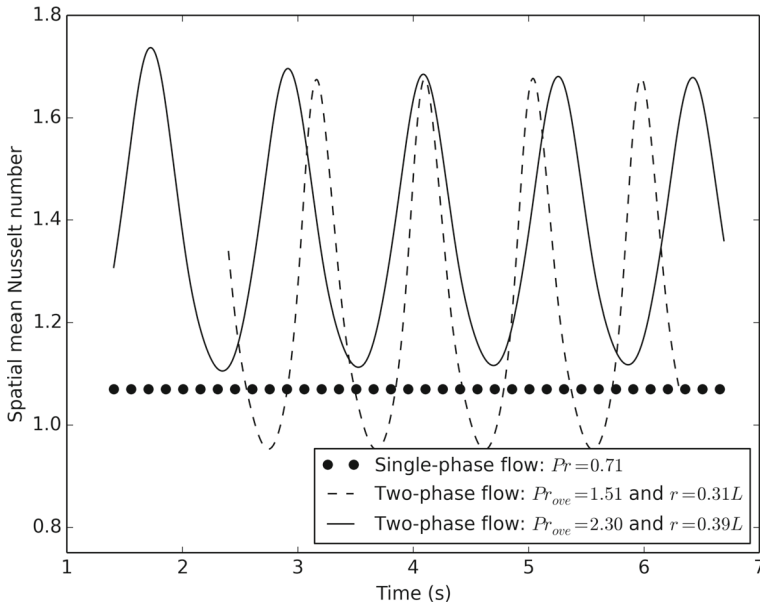
Fig. 11 Evolution of the spatial mean Nusselt number for the single-phase case ($Pr = 0.71$), two-phase flow with $r = 0.31L$ ($Pr_{ove} = 1.51$), and two-phase flow with $r = 0.39L$ ($Pr_{ove} = 2.30$)

of the dispersed phase in Fig. 10b compared to Fig. 10a intensified the impact of the Prandtl number on the temperature field. In general, the closer the dispersed phase was from the east wall, higher was the spatial mean Nusselt number at the east wall.

Figure 11 shows the temporal evolution of the spatial mean Nusselt number for the single-phase case ($Pr = 0.71$), the two-phase flow with $r = 0.31L$ ($Pr_{ove} = 1.51$), and the two-phase flow with $r = 0.39L$ ($Pr_{ove} = 2.30$).

According to Fig. 11, the spatial mean Nusselt number was intensified as the overall Prandtl number increased. Since the enlargement of the bubble radius increases the overall Prandtl number indirectly, it was expected that the simulation with the larger bubble would yield a larger thermal transfer rate compared to the simulation with the smaller radius. According to Fig. 11, the mean Nusselt number for the two-phase flows cases were severely altered from about -10.0% to almost $+60.0\%$ compared to the single-phase case. The thermal transfer rate was more enhanced in the simulation with the radius $0.39L$ compared to the simulation performed with the radius $0.31L$.

Table 7 summarizes the data related to the simulations treated in this subsection.

Table 7 Summary of the thermal transfer rate results to compute the effects of varying the overall Prandtl number and bubble radius

	$\bar{Nu}_{mean}$	$\bar{Nu}_{min}$	$\bar{Nu}_{max}$
Single-phase flow with $Pr = 0.71$	1.07	1.07	1.07
Two-phase flow with $Pr_{ove} = 1.51$ and $r = 0.31L$	1.23	0.95	1.67
Two-phase flow with $Pr_{ove} = 2.30$ and $r = 0.39L$	1.39	1.11	1.68

Table 7 presents a quantitative confirmation of the influence of the Prandtl number on the thermal transfer rate according to the calculated spatial mean Nusselt number. The spatial mean Nusselt number increased almost 30% and 15% by the addition of the dispersed phase with an initial radius of $0.39L$ and $0.31L$, respectively. Therefore, Table 7 confirms that the thermal transfer rate was enhanced as the overall Prandtl number of the flow mixture increased.

The influence of the overall Prandtl number may explain the reason why the literature has been reporting an increase of the thermal transfer rate at surfaces by the introduction of bubbles. Dabiri and Tryggvason [5] found that the bubbles's presence raised the Nusselt number at the heated wall, especially in the case with higher Prandtl number. The present paper is in acordance with Dabiri and Tryggvason [5] since the Prandtl number had a great impact on the thermal transfer mechanisms.

In the present paper, the closer the dispersed phase was to the heated wall, the higher was the spatial mean Nusselt number compared to the single-phase flow case. Similarly, the spatial mean Nusselt number increased in the simulations in which the distance between the bubbles and the wall were lower in Dabiri and Tryggvason [5].

As found by Dabiri and Tryggvason [5], when the dispersed phase was in the vinicity of the heated wall, the void fraction stirred up the viscous layer and reduced the size of the conduction region near the wall, improving the thermal transfer rate. In addition, when the dispersed phase was far from the heated wall, its influence was not significant and no improvement in the thermal transfer rate was observed.

8 Two-Phase Flow Simulations in which the Prandtl Number for the Dispersed Phase Was Lower than the Prandtl Number for the Continuous Phase

This section will present results for two-phase flows investigated in the situation where the Prandtl number for the dispersed phase is lower than the Prandtl number for the continuous phase. Three different analyses were performed, namely:

- $Pr_{dis} < Pr_{con}$ and the effects of overall Prandtl number variation were computed
- $Pr_{dis} < Pr_{con}$ and the effects of bubble size variation were evaluated
- $Pr_{dis} < Pr_{con}$ and the effects of simultaneous variations in the bubble size and overall Prandtl number were analyzed.

Section 8.1 presents the results of two-phase flow simulations with an initial bubble radius of $0.31L$ and overall Prandtl numbers 6.3 and 6.22. Section 8.2 will present the results of two-phase flow simulations with an overall Prandtl number of 6.22 and two bubble radii: $0.31L$ and $0.40L$. Section 8.3 will present the results of two-phase flow simulations with overall Prandtl numbers of 6.3 and 5.5 considering an initial bubble radius of $0.31L$ and $0.39L$, respectively.

8.1 Simulations with $Pr_{dis} < Pr_{con}$ and the effects of the overall Prandtl number variation

In this subsection, the results of two-phase flow simulations with an initial bubble radius of 0.31L will be presented. The Grashof number was taken equal to 1.4×10^4 and the continuous phase had Prandtl number 7.10. First, the Prandtl number for the dispersed phase was one-tenth that of the continuous phase ($Pr_{dis} = 0.71$ and $Pr_{con} = 7.10$ leading to

an overal Prandtl number of 6.30). Then, a simulation was performed considering a dispersed phase with Prandtl number only 1% that of the continuous phase ($Pr_{dis} = 0.071$ and $Pr_{con} = 7.10$ leading to an overal Prandtl number of 6.22).

Figure 12 shows the configuration of the isotherms in the two-phase flow cases with Gr=1.4×10^4 and $Pr_{ove} = 6.30$ a and $Pr_{ove} = 6.22$ b.

Figure 12 shows the configuration of the isotherms modified inside the dispersed phase. The isotherms inside the dispersed phase were more vertical than the isotherms seen in the figure for the single-phase case with $Pr = 7.1$ (Fig. 6b). The tendency of the isotherms to be more vertical was acentuated in the case with lower overall Prandtl number (Fig. 12b).

Figure 13 shows the temporal evolution of the spatial mean Nusselt number for the single-phase case ($Pr = 7.1$) as well as the two-phase flow cases with $Pr_{ove} = 6.3$ and $Pr_{ove} = 6.22$.

According to Fig. 13, the mean thermal transfer rate was reduced by the introduction of a bubble with lower Prandtl number than the continuous phase. The case with higher overall Prandtl number was associated to higher peaks of the spatial mean Nusselt number in comparison to the case with a lower overall Prandtl number.

Table 8 summarizes the results treated in the present subsection.

According to Table 8, the reduction of the thermal transfer rate was accompanied by a reduction of the overall Prandtl number. Since the overall Prandtl numbers from the two-phase flow cases were very similar, the thermal transfer rates between them were not significantly different. However, between the single-phase and two-phase cases, the influence of the overall Prandtl number is evident on the calculated thermal transfer rate.

8.2 Simulations with $Pr_{dis} < Pr_{con}$ and the effects of varying the bubble size

This subsection will present the results of two-phase flow simulations with initial bubble radii of $0.31L$ and $0.40L$. The Grashof number was taken equal to 1.4×10^4 and the continuous phase had a Prandtl number of 7.10. The overall Prandtl number was 6.22.

Figure 14 shows the temporal evolution of the spatial mean Nusselt number for the single-phase case ($Pr = 7.1$) as well as that for the two-phase flow cases ($Pr_{ove} = 6.22$) with $r = 0.31L$ and $r = 0.40L$.

(a)   (b)
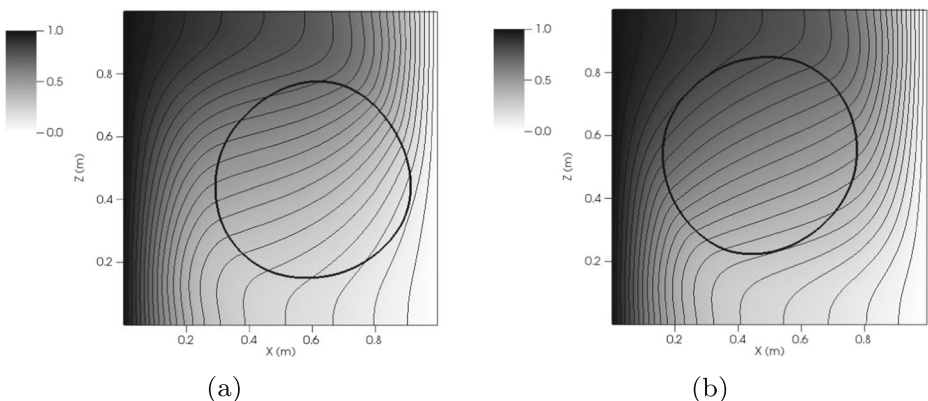
Fig. 12 Isotherms at central xz-plane for Gr=1.4×10^4, $Pr_{ove} = 6.30$ and $Pr_{ove} = 6.22$. The isotherms are represented with 20 thin isovalue contours. The thick contour represents the position of the interface. The temperature field is presented in grayscale
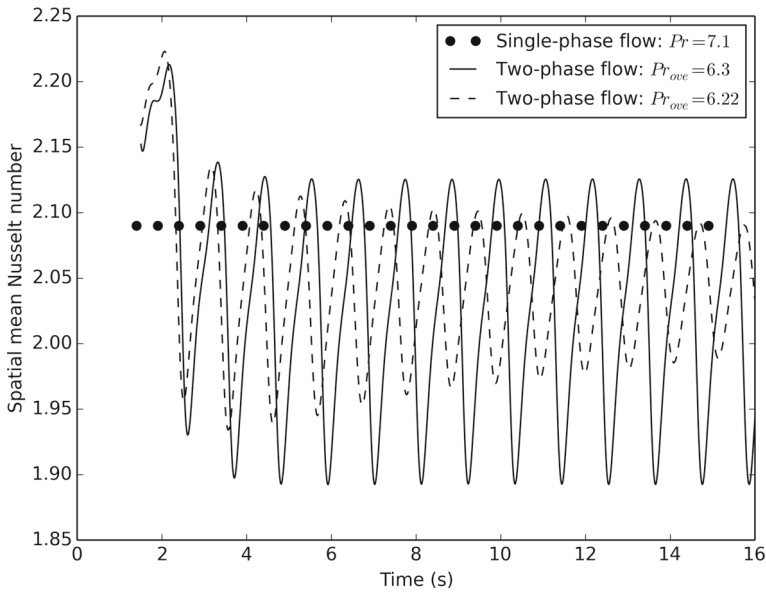
Fig. 13 Evolution of the patial mean Nusselt number for the single-phase case ($Pr = 7.1$) and the two-phase flows cases with $Pr_{ove} = 6.3$ and $Pr_{ove} = 6.22$

According to Fig. 14, the spatial mean Nusselt number varied in time for both cases ($r = 0.31L$ and $r = 0.40L$). The simulation with the bubble radius of $0.40L$ presented a more visible reduction of the thermal transfer rate compared to the case with a smaller bubble radius ($r = 0.31L$).

Table 9 shows the main results of the simulations presented in this subsection.

According to Table 9, the bubble radius influenced the thermal transfer rate. The larger bubble radius presented the lower mean, minimum and maximum thermal transfer rates in time. In the visual observations during the simulations, it was confirmed that, in general, the distance between the dispersed phase and the wall was lower, affecting the calculated value of the Nusselt number, similar to what was seen in the previous section. Therefore, the influence of the bubble radius was related to the proximity of the bubble to the wall during the bubble movement inside the domain.

8.3 Simulations with $Pr_{dis} < Pr_{con}$ and the effects of simultaneously varying the bubble size and overall Prandtl number

This subsection will present the results of two-phase flow simulations of natural convection considering $Gr = 1.4 \times 10^4$ and bubble initial radii of $0.31L$ and $0.39L$. The dispersed

Table 8 Summary of the thermal transfer rate results to compute the effects of varying the overall Prandtl number		$\bar{Nu}_{mean}$	$\bar{Nu}_{min}$	$\bar{Nu}_{max}$
	Single-phase flow with $Pr = 7.1$	2.09	2.09	2.09
	Two-phase flow with $Pr_{ove} = 6.3$	2.03	1.89	2.12
	Two-phase flow with $Pr_{ove} = 6.22$	2.03	1.98	2.09
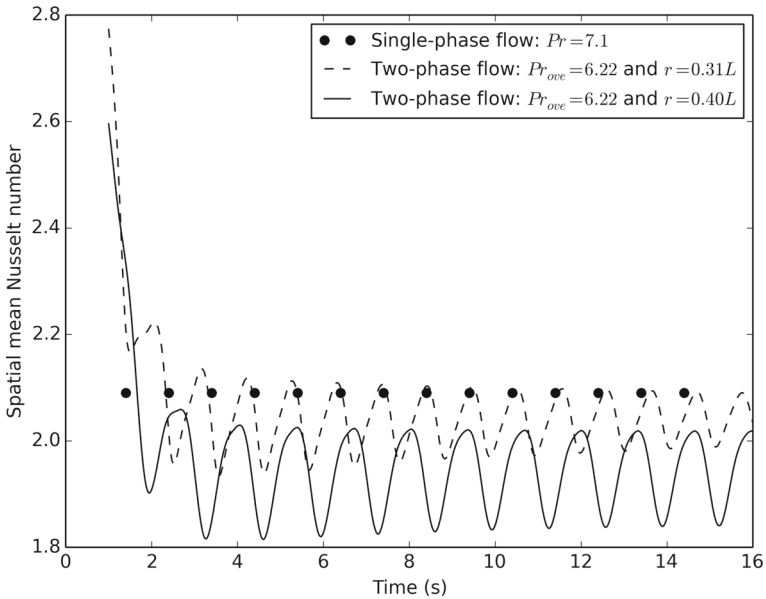
Fig. 14 Evolution of the spatial mean Nusselt number for the single-phase case ($Pr = 7.1$) and the two-phase flows cases with $Pr_{ove} = 6.22$ considering $r = 0.31L$ and $r = 0.40L$

phase had $Pr_{dis} = 0.71$ and the continuous phase $Pr_{con} = 7.1$. In addition, a simulation of single-phase flow was performed considering $Pr = 7.1$.

The overall Prandtl number of the two-phase flow simulation using an initial bubble radius of $r = 0.31L$ was 6.3 and the overall Prandtl number for the case with $r = 0.39L$ was 5.5. A similar simulation was conducted by Qiu et al. [8] using different initial radius for the dispersed phase.

Figure 15 shows the isotherms for the cases with $Pr_{ove} = 6.3$ and $Pr_{ove} = 5.5$.

According to Fig. 15, the isotherms presented a different pattern inside the dispersed phase compared to the single-phase flow. The isotherms inside the dispersed phase in Fig. 15 were less horizontal than the isotherms in the single-phase case, indicating the severe impact on the temperature field of the presence of the dispersed phase. The behavior of the isotherms inside the dispersed phase presented in the present paper are in accordance with the results of Qiu et al. [8], in which the isotherms inside the dispersed phase tended to be more vertical rather than horizontal.

Figure 15b illustrates the intensified effect previously seen in Fig. 15a due to the larger radius of the dispersed phase. The effect of the size of the radius on the thermal transfer rate was also reported by Qiu et al. [8], who reported a reduction in the mean Nusselt number as the radius of the dispersed phase was increased. Therefore, the thermal transfer rate and the

Table 9 Summary of the thermal transfer rate results to compute the effects of the bubble size variation with Grashof number equal to 1.4×10^4 and the overall Prandtl number was 6.22

|	$\bar{Nu}_{mean}$	$\bar{Nu}_{min}$	$\bar{Nu}_{max}$
Two-phase flow with $r = 0.31L$	2.03	1.98	2.09
Two-phase flow with $r = 0.40L$	1.96	1.84	2.01
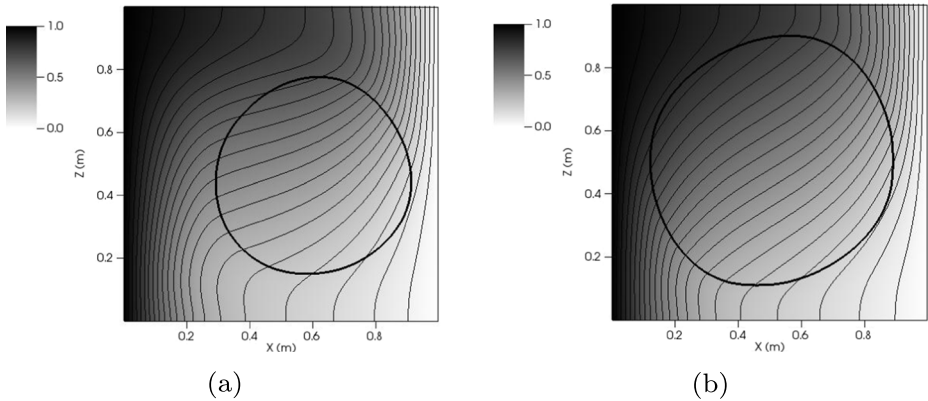
Fig. 15 Isotherms at central xz-plane for Gr=1.4×10^4, $Pr_{ove} = 6.3$ (**a**) and $Pr_{ove} = 5.5$ (**b**). The isotherms are represented with 20 thin isovalue contours. The thick contour represents the interface position. The temperature field is presented in grayscale

overall Prandtl number of flow mixture have a straightforward connection, as demonstrated in the former sections.

Figure 16 shows the evolution in time of the spatial mean Nusselt number for the single-phase case ($Pr = 7.1$), the two-phase case with $Pr_{ove} = 6.3$, and the two-phase case with $Pr_{ove} = 5.5$.

According to Fig. 16, the spatial mean Nusselt number was directly affected by varying the overall Prandtl number. The increase of the bubble radius intensified the importance of the Prandtl number for the dispersed phase, reducing even more the Nusselt number.
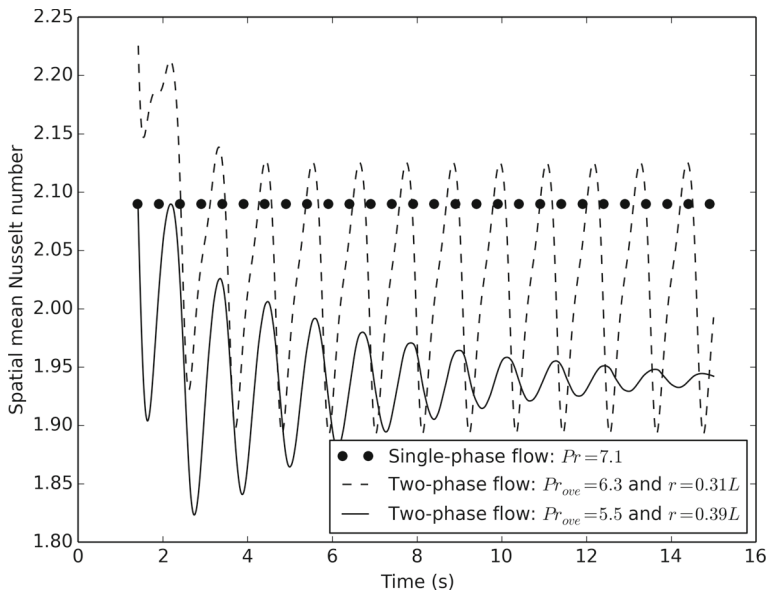
Fig. 16 Evolution of the spatial mean Nusselt number for the single-phase case ($Pr = 7.1$) and two-phase flows cases with a dispersed phase with radii of $0.31L$ ($Pr_{ove} = 6.3$) and $0.39L$ ($Pr_{ove} = 5.5$)

Table 10 Summary of the thermal transfer rate results to compute the effects of varying the overall Prandtl number and the bubble radius

	$\bar{N}u$	$\bar{N}u_{min}$	$\bar{N}u_{max}$
Single-phase flow with $Pr = 7.1$	2.09	2.09	2.09
Two-phase flow with $Pr_{ove} = 6.3$ and $r = 0.31L$	2.03	1.89	2.12
Two-phase flow with $Pr_{ove} = 5.5$ and $r = 0.39L$	1.94	1.93	1.95

According to Fig. 16, the spatial mean Nusselt number at the east wall presented values from about $+2\%$ to almost -12% compared to the single-phase case. The results reported in Fig. 16 demonstrate the decrease in the spatial mean Nusselt number when the dispersed phase was in the vinicity of the heated wall; the thermal transfer rate increases when the dispersed phase moved far away from the heated wall. The maximum value of the Nusselt number was approximately the value from the single-phase case, since the dispersed phase has little influence on the thermal transfer rate when it is away from the heated wall.

Figure 16 presents an example of the case where the addition of a dispersed phase did not enhance the thermal transfer rate at a surface in contact with a two-phase flow. In fact, the results presented in Fig. 16 show the severe reduction of the spatial mean Nusselt number in the two-phase flow cases compared to the single-phase case. In addition, Fig. 16 illustrates the intensification of the influence of the overall Prandtl number on the thermal transfer rate in the case where the radius of the dispersed phase was larger. Therefore, the overall Prandtl number of the flow mixture and the bubble radius control the reduction of the thermal transfer rate in Fig. 16, since the tendency observed for the case with the bubble initial radius of $0.31L$ was more evident for the case where the initial bubble radius was $0.39L$.

Table 10 presents the influence of the overall Prandtl number and the bubble radius on the thermal transfer rate using the spatial mean Nusselt number at the east wall.

Table 10 presents the effects of the overall Prandtl number of the flow mixture on the spatial mean Nusselt number calculated at the heated wall. As the overall Prandtl number of the flow mixture decreases, the mean Nusselt number decreases. In accordance with a similar simulation performed by Qiu et al. [8], it was found that the thermal transfer rate decreased as the bubble radius increased. The variation of the Nusselt number compared to the single-phase flow case presented in Table 10 goes against the generally accepted hypothesis that the Nusselt number increases with the introduction of bubbles in single-phase flows.

Based on the results from Dabiri and Tryggvason [5], the authors of the present paper believe in the intensification of the reduction of the Nusselt number presented in Table 10 if the distance between the walls and the dispersed phase is lower. Finally, this last section has provided several results refuting the argument generally seen in the literature that the introduction of bubbles necessarily increases the wall-to-fluid thermal transfer rate. Future research needs to be conducted in order to analyze new factors related to this topic, such as the influence of the bubble shape on the thermal transfer rates.

9 Conclusions

The research presented in this paper conducted a detailed qualitative and quantitative analysis of the influence of the bubble radius size and the overall Prandtl number on the wall-to-fluid thermal transfer rate in two-phase flow in a cubic cavity. According to the

results obtained here, the overall Prandtl number and the bubble radius size contributed to changes in the Nusselt number in the classical problem of a differentially heated cavity.

The Prandtl number is found to be a crucial parameter for evaluating thermal transfer rates in two-phase flows in cavities since the overall Prandtl number of the mixture of fluids controlled the increase or decrease of the thermal transfer rate compared to the single-phase flows. In addition, the bubble radius size affected the pattern of bubble movement inside the cavity, which changed the proximity between the dispersed phase and the heated walls modyfing the local thermal transfer rate.

Finally, the presence of a dispersed phase did not in itself increase the wall-to-fluid thermal transfer as previously stated in the literature; however, the Prandtl number of the flow mixture affects the variations of the local and the mean thermal transfer rate.

The results obtained in the present paper may guide future works on more complex physical problems related to two-phase flows since it was restricted to the configuration of a cubic cavity and some physical assumptions were assumed, Finally, the authors of the present paper suggest future investigations on the effects of the Prandtl number combined with other flow characteristics, such as bouyancy, bubble shape or modelling multiples bubbles.

Compliance with Ethical Standards

Conflict of interests   The authors declare that they have no conflict of interest.

References

1. Deen, N., Kuipers, J.: Direct numerical simulation of wall-to liquid heat transfer in dispersed gas-liquid two-pahse flow using a volume of fluid approach. Chem. Eng. Sci. **102**, 268–282 (2013). https://doi.org/10.1016/j.ces.2013.08.025
2. Deckwer, W.D.: On the mechanism of heat transfer in bubble column reactor. Chem. Eng. Sci. **92**, 1341–1346 (1980). https://doi.org/10.1016/0009-2509(80)85127-X
3. Oresta, P., Verzicco, R., Lohse, D., Prosperetti, A.: Heat transfer mechanisms in bubbly Rayleigh-Bénard convection. Phys. Rev. **80**, 259–293 (2007). https://doi.org/10.1103/PhysRevE.80.026304
4. Tamari, M., Nishikawa, K.: The stirring effect of bubbles upon the heat transfer to liquids. Heat Transfer – Japonese Res. **5**, 31–44 (1976). https://doi.org/10.1299/kikai1938.33.87
5. Dabiri, S., Tryggvason, G.: Heat transfer in turbulent bubbly flow in vertical channels. Chem. Eng. Sci. **122**, 106–113 (2015). https://doi.org/10.1016/j.ces.2014.09.006
6. Bukhari, S., Siddiqui, M.: Characteristics of air and water velocity fields during natural convection. Heat Mass Transfer **43**, 415–525 (2007). https://doi.org/10.1007/s00231-005-0072-8
7. Chandra, A., Chhabra, R.P.: Effect of prandtl number on natural convection heat transfer from a heated semi-circular cylinder. Int. J. Mech. Aerosp. Ind. Mechatron. Manuf. Eng. **6**, 106–113 (2012). https://doi.org/10.1016/j.ces.2014.09.006
8. Qiu, R., Wang, A., Jiang, T.: Lattice boltzmann method for natural convection with multicomponent and multiphase fluids in a two-dimensional square cavity. Canad. J. Chem. Eng. **92**, 1121–1129 (2014). https://doi.org/10.1002/cjce.21950
9. Wan, D., Patnaik, B., Wei, G.: A new benchmark quality solution for the buoyancy-driven cavity by discrete singular convolution. Numer. Heat Transfer **40**, 199–228 (2001). https://doi.org/10.1080/104077901752379620
10. Kizildag, D., Rodríguez, I., Oliva, A., Lehmkuhl, O.: Limits of the oberbeck-boussinesq approximation in a tall differentially heated cavity filled with water. Int. J. Heat Mass Transfer **68**, 489–499 (2014). https://doi.org/10.1016/j.ijheatmasstransfer.2013.09.046
11. White, F.M.: Viscous Fluid Flow. McGraw-Hill (1974)

12. Wang, P., Zhang, Y., Guo, Z.: Numerical study of three-dimensional natural convection in a cubical cavity at high rayleigh numbers. Int. J. Heat Mass Transf. **113**, 217–228 (2017). https://doi.org/10.1016/j.ijheatmasstransfer.2017.05.057

13. Brackbill, J.U., Kothe, D.B., Zemach, C.: A continuum method for modeling surface-tension. J. Comput. Phys. **100**, 335–354 (1992). https://doi.org/10.1016/0021-9991(92)90240-Y

14. Chorin, A.J.: Numerical solution of the Navier–Stokes equations. Math. Comput. **22**, 745–762 (1968). https://doi.org/10.1090/s0025-5718-1968-0242392-2

15. Centrella, J.M., Wilson, J.R.: Planar numerical cosmology. II - the difference equations and numerical tests. Astrophys. J. Suppl. Series **54**, 229–249 (1984). https://doi.org/10.1086/190927

16. Germano, M., Piomelli, U., Moin, P., Cabot, W.H.: A dynamic subgrid-scale eddy viscosity model. Phys. Fluids A: Fluid Dyn. **3**, 1760–1765 (1991)

17. Lilly, D.: A proposed modification of the germano subgrid-scale closure method. Phys. Fluids A: Fluid Dyn. **4**, 633 (1992)

18. Akhtar, M., Kleis, S.: Boiling flow simulations on adaptive octree grids. Int. J. Multiphase Flow **53**, 88–99 (2013). https://doi.org/10.1016/j.ijmultiphaseflow.2013.01.008

19. Hirt, C.W., Nichols, B.D.: Volume of fluid (vof) method for the dynamics of free boundaries. J. Comput. Phys. **39**, 201–225 (1981). https://doi.org/10.1016/0021-9991(81)90145-5

20. Wachem, B.G.M., Schouten, J.C.: Experimental validation of 3-d lagragian vof model: Bubble shape and rise velocity. AIChE J **48**, 253–282 (2002). https://doi.org/10.1002/aic.690481205

21. Dennner, F., Wachem, B.G.M.: Fully-coupled balanced-force vof framework for arbitrary meshes with least-squares curvature evaluation from volume fractions. Numer. Heat Transfer Part B: Fund. **65**, 218–255 (2014). https://doi.org/10.1080/10407790.2013.849996

22. Barbi, F., Pivello, M.R., Villar, M.M., Serfaty, R., Roma, A.M., Silveira-Neto, A.: Numerical experiments of ascending bubbles for fluid dynamic force calculations. J. Braz. Soc. Mech. Sci. Eng. **40**, 519–531 (2018). https://doi.org/10.1007/s40430-018-1435-7

23. Krane, R.J., Jessee, J.: Some detailed field measurements for a natural convection flow in a vertical square enclosure. Proc. First ASME-JSME Thermal Eng. Joint Conf. **1**, 323–329 (1983)

24. Padilla, E., Lourenço, M., Silveira-Neto, A.: Natural convection inside cubical cavities: Numerical solutions with two boundary conditions. J. Braz. Soc. Mech. Sci. Eng. **35**, 275–283 (2013). https://doi.org/10.1007/s40430-013-0033-y